Journal of Structural Geology, Vol. 12, No. 5/6, pp. 785 to 794, 1990
Printed in Great Britain

0191-8141/90 $03.00+0.00
Pergamon Press plc

Dislocation enhanced selective dissolution: an examination of mechanical aspects using deformation-mechanism maps

A. MEIKE*

Materials and Chemical Sciences Division, Lawrence Berkeley Laboratory, University of California, Berkeley, CA 94720, U.S.A.

(*Received* 10 *February* 1989; *accepted in revised form* 1 *December* 1989)

Abstract—Analysis of dislocation configuration energetics reveals that free dislocations are responsible for the greatest strain energy per unit volume. Further interpretation suggests that pile-ups of free dislocations, called the dislocation enhanced selective dissolution (DESD) microstructure, have the greatest potential for selective dissolution. These mechanical arguments are identical for phase transformations activated by dislocation strain. The DESD microstructure is characteristic of low dislocation mobility and need not produce macroscopic evidence of strain. Therefore a DESD field is proposed for relatively low homologous temperature and shear stress on a deformation mechanism map. An exploration of the effects of solution-transfer deformation in a polymineralic assemblage via dislocation mechanism maps suggests that DESD has the potential to produce more anisotropic textures than pressure solution.

INTRODUCTION

NON-HYDROSTATIC stress drives a range of reaction mechanisms. These include phase transitions caused by martensitic transformation, dissolution driven directly by a stress gradient, and phase transitions and dissolution that are secondary consequences of shear accommodation mechanisms, such as dislocations (e.g. Sorby 1863, Weyl 1959, Kamb 1961, Coe & Paterson 1969, Newton *et al.* 1969, Coe 1970, Durney 1972, Elliot 1972, Green 1972, Paterson 1973, Kerrich *et al.* 1977, McClay 1977, Green 1980, Poirier 1981, Vaughan *et al.* 1984, Kerrick 1986). As a result, the effect of non-hydrostatic stress on minerals can be complex. The intent of this paper is to clarify, from a micromechanical perspective, the conditions that favor dislocation-activated reactions.

At present, our micromechanical knowledge of important rock-forming minerals is incomplete. However, we have a good general knowledge of the micromechanics of flow from the metallurgical literature. Polycrystalline materials deform by one of a few independent flow mechanisms that include obstacle- or lattice-controlled plasticity, power-law creep and diffusional flow. Each flow mechanism can be described by a constitutive strain-rate equation, also called a flow law, and can be associated with a characteristic steady-state microstructure. Deformation-mechanism maps (Frost & Ashby 1982) plot the dominant strain-rate controlling mechanism as a function of normalized state variables such as shear stress and temperature or grain size and temperature. Isomechanical materials can be found for which the field boundaries are more or less indistinguishable. The field boundaries change between isomechanical groups, but the relative positions of the fields are constant. For example, flow driven by lattice mechanisms is always found at the high homologous shear-stress side of the diagram, and flow driven by boundary-diffusion mechanisms at the low homologous shear-stress side. Here the utility of the maps is clear. Flow regimes, identified by characteristic microstructures, can be compared. Thus relationships between mechanisms of poorly characterized materials can be explored by analogy to a more thoroughly understood isomechanical material.

The DESD mechanism probably becomes more significant under conditions that favor a specific microstructure, analogous to characteristic microstructures of other flow mechanisms. This study identifies that microstructure based on the assumption that it must represent a maximum strain energy density for a given dislocation line length. A DESD field is defined on a deformation-mechanism map in order to allow the exploration of textural consequences for a polymineralic aggregate.

DISLOCATION DYNAMICS AND CONFIGURATIONAL ENERGETICS

A dislocation is a crystal discontinuity described by the Burgers vector, **b**, whose magnitude is the offset, b. It activates from a grain boundary or an internal defect as a row of broken atomic bonds, and moves into the crystal by progressively breaking and re-establishing bonds (Fig. 1c). Those dislocations activated by the same sense of shear have the same sign. The total energetic contribution of dislocations can be inventoried as the surface free energy of the discontinuity ($\Delta G_{surface}$), and the volumetric strain energy (ΔG_{strain}) due to an elastic displacement of the crystal structure about the discontinuity.

Recent investigations of the effect of dislocations on mineral dissolution are being pursued both in experiment (Brantley *et al.* 1986, Casey *et al.* 1988, Murphy

*Present address: Earth Sciences Department, L-219, Lawrence Livermore National Laboratory, Livermore, CA 94550, U.S.A.

1989) and theory (Helgeson *et al.* 1984, Wintsch & Dunning 1985, Lasaga & Blum 1986). The most familiar forms of these equations are found as models of etch pit growth (Frank 1951, Cabrera *et al.* 1954, Cabrera & Levine 1956, Bennema & Van Enckevort 1979, Van der Hoek *et al.* 1982). Although the strain energy contribution of a dislocation is due to an elastic displacement, unlike reversible elastic strain the effects of multiple increments are not additive because the strain fields of the dislocations interact. Dislocations of like sign repel each other at less than a threshold distance, and attract at distances greater. The converse is true of dislocations of opposite sign, which can thus annihilate each other. Therefore, even though dislocations are not equilibrium microstructures, given enough mobility they tend to organize into lower energy configurations. As a consequence, dislocation microstructures are not energetically equivalent.

The configurational energetics of a range of microstructures will be analyzed below for a mole of a hypothetical garnet. The steady-state microstructures representative of the range of lattice mechanisms are considered with reference to a general deformation-mechanism map (Fig. 2), which is represented on axes of normalized shear stress (τ/μ) and normalized temperature (T/T_m). The normalization parameters are the shear modulus (μ) and the melting temperature (T_m). For the purpose of comparison, we attribute the energetic differences between microstructures completely to

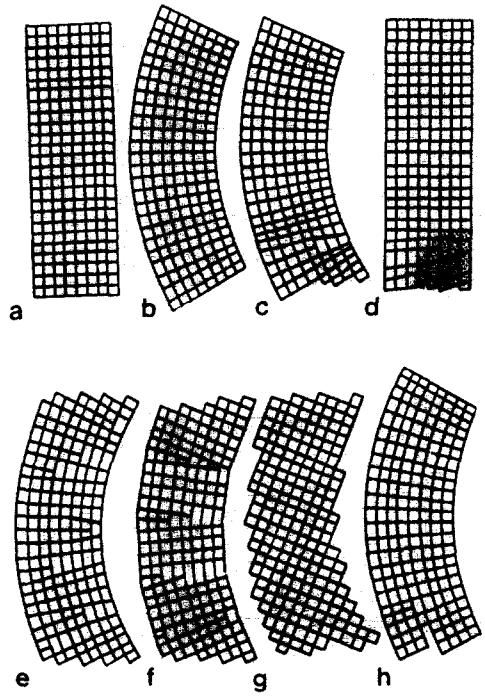

Fig. 1. States of strain in a single crystal, exaggerated for illustration. (a) Undeformed. (b) Microscopic elastic strain. (c) Microscopic permanent deformation. Dislocations activate when the shear stress resolved on a slip system exceeds the dislocation-activation stress. (d) Macroscopic elastic strain. Microscopic permanent deformation can be present. The stippled region marks a DESD site. (e) Homogeneously distributed dislocations. (f) Polygonized dislocations. (g) Annealed crystal. Macroscopic strain is permanent, but the crystal is perfect. No dislocation strain exists. (h) Fracture. On a microscopic scale a fracture represents a linear array of dislocations.

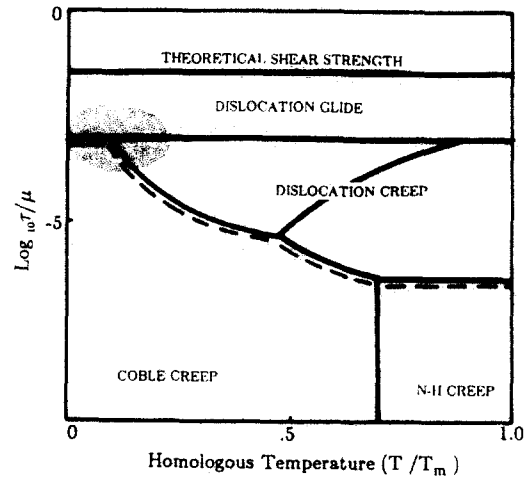

Fig. 2. A diagram of a generalized deformation-mechanism map illustrates the relationships between the steady-state flow regimes on axes of normalized temperature (T/T_m) and normalized shear stress (τ/μ), where T_m represents the melting temperature and μ represents the shear modulus. The broken line indicates the boundary between lattice- and boundary-diffusion mechanisms. The stippled region represents the proposed DESD regime.

ΔG_{strain}, independent of $\Delta G_{surface}$, although it may be necessary to consider it in the future.

The volume of crystal that surrounds the discontinuity can be viewed as an elastically distorted cylinder. The strain-energy contribution of the distortion is usually modeled by two methods. The outer volume of the cylinder defined by the effective dislocation radius R and a cutoff radius r_0, can be described adequately by a continuum elastic approach. The elastic strain energy of the dislocation core, the volume between r_0 ($\approx 10^{-7}$ cm for metals) and the discontinuity, cannot be determined by this method, but rather requires an atom by atom evaluation (e.g. Puls 1981, Bacon & Martin 1982, Bucher 1982). The significance of the core energy to dissolution is not yet well established. The standard estimate of core energy (Cottrell 1953), roughly one-tenth of the strain energy per unit line length, suggests that a core energy could be neglected for a first-order approximation. In addition, the core energy for the same dislocation line length may not vary from one microstructure to the next, and may therefore be omitted for the purpose of microstructural evaluation. A significant core contribution, on the other hand, reflects the same self stress field exhibited by the outer volume and can therefore only reinforce its effects. Therefore, for the sake of simplicity, only the contribution of the outer volume is evaluated below.

The standard continuum elastic estimate of strain energy per unit line length (η) of a dislocation is derived by integration over the cylindrical volume of crystal around the dislocation. The resultant isotropic infinite crystal approximation:

$$\eta = \frac{\mu b^2}{4\pi K}(\ln R/r_0) \qquad (1)$$

(Cottrell 1953, p. 38) will be used to compare dislocation configurations in this paper. The standard estimate of η as μb^2, where μ respresents the shear modulus, is clear

from this equation. Modification of the logarithmic term to $(\ln R/r_0 - 1)$ accounts for the absence of stress at the surface of a finite crystal, and is easily verified from the origin equations. As will be discussed below, the standard approximation $R = \rho^{1/2}$, where ρ represents an experimentally determined dislocation density, implicitly defines a microstructure. The strain symmetry is defined by K, which has a value of 1 for screw dislocations and $1 - \nu$ for edge dislocations, where ν represents the Poisson's ratio.

Parameters for almandine rich garnet (Ia3d) (Table 1) are collected from Birch (1966) and Smith (1982). It is standard practice to use the isotropic approximation for cubic crystals. For this garnet, the anisotropy ratio $A = 2c_{44}/c_{11} - c_{12} = 0.98$, where an A is a function of elastic constants (c_{ij}), and 1 represents perfect isotropy. Therefore, the isotropic approximation is appropriate for the calculations below. Here the material parameter $\mu b^2/4\pi K$ modified by the molar volume, V_m, is represented as Φ in the equations for ΔG_{strain} that follow. The value of Φ is constant for a single dislocation type and material. Substitution of the garnet parameters yields a Φ of 2.04×10^{-9} cal-cm^2 mol^{-1} for perfect screw dislocations, and 2.79×10^{-9} cal-cm^2 mol^{-1} for perfect edge dislocations. The general consensus from experimental and theoretical work is that dislocation densities of approximately 10^{10} cm^{-2} are necessary for the onset of significant reactions activated by dislocation strain (e.g. Wintsch & Dunning 1985, Brantley *et al.* 1986, Kerrick 1986, Lasaga & Blum 1986). A density of 5×10^{10} cm cm^{-3} is chosen for the calculations below.

Dislocations are confined to two-dimensional glide planes at great shear stresses. The interaction between strain fields compels dislocations with enough mobility to space themselves regularly along the glide planes. The resultant slip bands are characteristic of the dislocation-glide regime (Fig. 2). Suppose a dislocation density (ρ) of 5×10^{10} cm cm^{-3} is distributed homogeneously throughout a crystal (Fig. 1e). We can then argue that the approximation $R = \rho^{1/2}$ is appropriate. Equation (1) yields a strain energy contribution per mole of garnet:

$$\Delta G_{strain} = \Phi \ln (4.5 \times 10^{-6}/10^{-7})(5 \times 10^{10}) \quad (2)$$
$$= 388 \text{ cal mol}^{-1} \text{ screw dislocations}$$
$$= 531 \text{ cal mol}^{-1} \text{ edge dislocations.}$$

Table 1. Physical parameters for a hypothetical almandine garnet employed in the stress–strain calculations at 25°C

Parameter	Value
$a\langle 111\rangle$ screw	0.993 nm*
$a\langle 100\rangle$ edge	1.147 nm*
μ	c_{44} = 94.4 GPa†
ν	$c_{12}/(c_{11} + c_{12}) = 0.269$
r_0	10^{-7} cm
c_{11}	3.05×10^2 GPa†
c_{12}	1.12×10^2 GPa†
c_{44}	94.4 GPa†
V_m	115.1 cm^3 mol^{-1}*

*From Smith (1982).
†Almandite, from Birch (1966).

At moderate homologous temperatures and lower shear stresses, a dislocation is able to climb from its glide plane, which facilitates obstacle circumvention. This increased freedom of movement allows dislocations to polygonize (see Cahn 1985) as represented by the sequence (e) → (f) (Fig. 1), which is the characteristic microstructure of the dislocation creep regime (Fig. 2). As discussed by Nabarro (1967, p. 76) a twist boundary composed of screw dislocations produces no long range strain and will not be considered. The strain energy per unit area of a tilt boundary, a dislocation wall composed of edge dislocations, has been described as:

$$\eta_W = \Phi \ln (R/r_0)(1/2R) \quad (3)$$

(Nabarro 1967, p. 77). Consider prismatic subgrains of dimensions: 0.125 μm^3. The area of dislocation wall is then $\approx 6 \times 10^4$ cm^2 cm^{-3}. A dislocation line length 5×10^{10} cm cm^{-3}, spaced evenly along that wall, would be separated by a distance of $\approx 1.2 \times 10^{-6}$ cm, and thus has an effective radius of $R = 6.0 \times 10^{-7}$ cm. In this case the dislocation strain energy for a mole of garnet is calculated to be:

$$\Delta G_{strain} \quad (4)$$
$$= \Phi \ln (6.0 \times 10^{-7}/10^{-7})(1/1.2 \times 10^{-6})(6.0 \times 10^4)$$
$$= 250 \text{ cal mole}^{-1} \text{ tilt boundary.}$$

The calculated strain energy of this wall is less than half that of the same length of free edge dislocations. The elastic strain falls off rapidly with distance from the dislocation walls (Nabarro 1967, p. 76). Thus dissolution in the case of a dislocation wall is a two-dimensional, not volumetric, effect. In general, the strain energy of organized dislocation microstructures will be lower than that of free dislocations of the same density. Inspection of equation (3) indicates that increased organization of the dislocations and the concomitant reduction of R allows the logarithmic term, $\ln (R/r_0)$ to approach zero. As the proximity of the dislocations increases, the angle of orientation increases, and the dislocation strain fields overlap. Generally, beyond a 10–15° misorientation, individual dislocations lose their identity (Porter & Easterling 1982, p. 118) and coherence across the wall is lost. Consequently, the strain-energy contribution to the total energy of the system approaches zero. However, the total effect of polygonization on free energy is complex because the ultimate decrease in the effective grain size increases the effective surface area, and thus the $G_{surface}$ contribution.

Low temperature limits dislocation mobility. Under these conditions dislocations pile up behind obstacles, or remain close to their source because lattice energy is too great (Peierls stress, see Peierls 1940, Nabarro 1967). Suppose the same 5×10^{10} cm cm^{-3} length of dislocation line is concentrated into a tenth of the crystal volume (Fig. 1d). Most standard methods average dislocation density over a relatively large volume, which in this case would result in a value of 5×10^9 cm cm^{-3}. If we were to assume erroneously that $R = \rho^{-1/2}$. The calculated strain-energy contribution for a mole of garnet would be:

$$\Delta G_{strain} = \Phi \ln (1.4 \times 10^{-5}/10^{-7})(5 \times 10^{9}) \quad (5)$$
$$= 50 \text{ cal mol}^{-1} \text{ screw dislocations}$$
$$= 69 \text{ cal mol}^{-1} \text{ edge dislocations}$$

which is significantly different from the actual state. The crystal contains regions of perfect structure ($\Delta G_{strain} = 0$) that coexist with regions that are as reactive as the case described in equation (2) ($\Delta G_{strain} = 531$ cal mol^{-1}). However, unlike the previous homogeneous case, dissolution would be selective (stipple, Fig. 1d). Comparison of equation (5) with equation (2) illustrates the decrease in the energetic difference between screw and edge dislocations with decreasing density.

In sum, free dislocations contribute the greatest configurational strain energy and are therefore the primary candidates for dislocation-activated reactions. Dislocation organization can reduce and even nullify the strain-energy potential of free dislocations. Therefore, to approximate R as $\rho^{-1/2}$, which implicitly assumes that dislocation microstructures are composed of free dislocations, may result in an overestimate of the actual strain energy of the system. Pile-ups of free dislocations, which will be called the DESD microstructure in the discussion that follows, offer the greatest potential for a selective effect.

APPLICATION TO DEFORMATION MECHANISM MAPS

Experimental critical resolved shear stress (CRSS) values are frequently used to estimate a threshold stress for dislocation-enhanced dissolution strain because, according to conventional thought, CRSS is required to generate a significant density of dislocations. The standard working definition of CRSS (Schmid 1924, Poirier 1985) is measurable plastic deformation, or plastesis, even though at times the theoretical definition of CRSS approaches an atomic scale (Cottrell 1953). Therefore the CRSS threshold assumption is equivalent to an assumption that the extent of plastic deformation is directly proportional to the potential for DESD strain. An examination of dislocation dynamics proves that this is not the case. Ductile strain is caused by dislocation movement through the crystal and annihilation at the opposite boundary, represented by the sequence (a) ⇒ (b) ⇒ (c) ⇒ (e) ⇒ (f) ⇒ (g) (Fig. 1). In contrast, dislocations function passively in DESD strain. Permanent shape change occurs if a sufficient density of dislocations is accessible to fluids as illustrated by the sequence (a) ⇒ (b) ⇒ (c) ⇒ (d) (Fig. 1). Consequently, DESD does not not require the dislocation mobility that is implicit in the experimental values of CRSS. In fact dislocation organization and annihilation reduces dislocation density (Fig. 1g) and thus the potential for DESD. These considerations suggest that the threshold stress for DESD is lower than the experimentally determined values of CRSS.

Like elastic deformation illustrated by the sequence (a) ⇒ (b) ⇒ (a), DESD results in a macroscopically unstrained crystal (Fig. 1d). However, in the latter case dislocations are activated. The result is not microscopically elastic. Therefore, the DESD microstructure has the greatest potential to transform a crystal from macroscopically 'unstrained' to macroscopically 'strained' in the presence of fluid. Dislocations have a negligible volumetric effect on a crystal (Clarebrough *et al.* 1957, Keyes 1958) and great densities do not necessarily cause macroscopic plastic deformation. Clusters of dislocations dense enough to significantly enhance dissolution (10^{9}–10^{10} cm cm^{-3}) have been observed in experimentally and naturally stressed calcite (Meike 1988, Meike & Wenk 1988) that show no macroscopic evidence of ductile strain. Consistent with the considerations above, the experimental samples underwent maximum shear stresses far below the appropriate CRSS value. It is clear that the threshold stress for DESD should be defined on submicroscopic criteria such as dislocation-activation stresses, which are as yet unknown for rock forming minerals.

The low dislocation mobility required for the DESD microstructure is similar to cold-working in metals. Cold-working can occur at low homologous temperatures and shear stresses, consistent with the calcite observations mentioned above. For the sake of discussion, by analogy to cold-working a DESD field can be located at the low-temperature end of the dislocation-glide field of a deformation-mechanism map at the triple point between the glide, Coble creep and dislocation-creep fields (stipple, Fig. 2). However, over geologic time spans one could argue that the field extends the length of the boundary between lattice- and boundary-diffusion mechanisms (broken line, Fig. 2). As should be apparent from the discussion of CRSS above, the actual position of the DESD field depends on the resolution of the measurement used to determine the boundary. A more critical determination of the extent of the DESD field also involves consideration of the dissolution rate with respect to the rate of dislocation activation, and thus depends on the identity of the mineral.

The propriety of representing a DESD field on a dry steady-state deformation-mechanism map may be questioned from two perspectives. First, the analogy between DESD and cold-working microstructures ultimately may be pursued more rigorously on transient-state deformation-mechanism maps, which are plotted on the same axes, but contoured in cumulative strain (Frost & Ashby 1982). However, since the arguments for the location of the DESD field would be identical, and no transient state maps of rock-forming minerals are available, steady-state maps are used. In addition, although cold-working is considered a transient mechanism, it is possible that on a geological time scale a balance between dissolution and dislocation-activation rates could result in a quasi-steady-state DESD microstructure (Fig. 1h). Second, although suitable for phase transformations activated by dislocation strain, it may seem inappropriate to represent a DESD field on a dry deformation-mechanism map. However, only the quali-

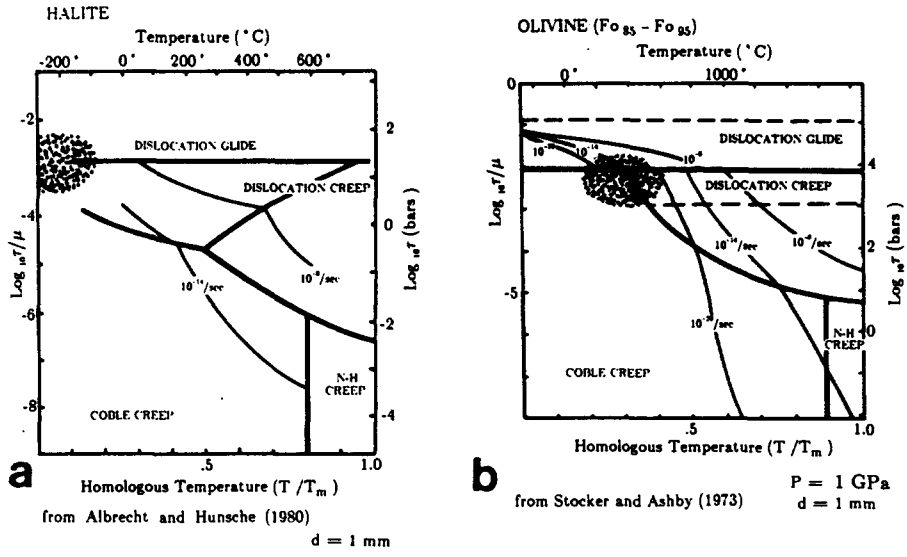

Fig. 3. Deformation-mechanism maps for 1 mm diameter aggregates of (a) halite (from Albrecht & Hunsche 1980) at ≈1 bar and (b) olivine (Fo_{85}—Fo_{95}) (from Stocker & Ashby 1973) at ≈1 GPa. The stippled area represents the proposed DESD field which would be found in halite at temperatures below 0°C and shear stresses of a single order or magnitude, and in olivine (P_c = 1 GPa) at roughly 400–600°C and two or three orders of magnitude greater shear stress.

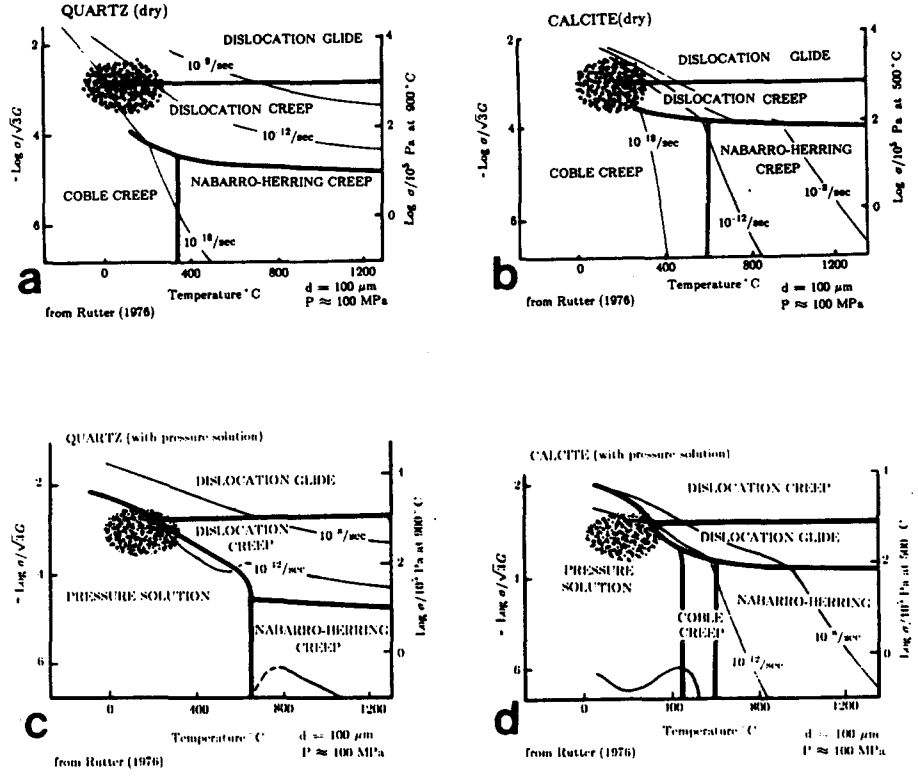

Fig. 4. Dry deformation-mechanism maps for (a) quartz and (b) calcite from Rutter (1976). A grain size of 100 μm and a confining pressure of 100 MPa were inferred from Rutter's appendices. The stippled area illustrates the location of the DESD field at roughly 200°C and $10^{2-2.5}$ MPa. Deformation-mechanism maps that include a pressure-solution field for (c) calcite and (d) quartz. The stippled DESD field is superimposed.

tative aspects, such as the relative position of the DESD field with respect to other fields can be pursued with the present available data. These relative relationships will not change in the presence of water.

Comparison of deformation-mechanism maps for a 1 mm grain size of representative minerals from either end of the stiffness spectrum, halite (Albrecht & Hunsche 1980) (Fig. 3a) and olivine (Fo_{85}–Fo_{95}) (Stocker & Ashby 1973) (Fig. 3b) suggests that DESD (illustrated in stipple) would be found under widely disparate conditions. In halite, DESD would be found at temperatures below 0°C and shear stresses of a single order of magnitude. In olivine, on the other hand, DESD would operate at 400–600°C and two or three orders of magnitude greater shear stress. More qualitative maps of quartz (Fig. 4a) and calcite (Fig. 4b) (Rutter 1976), illustrate the location of the DESD field at approximately $10^{2.5}$ MPa, 200°C, and 10^2 MPa, 200°C, respect-

ively. The 100 μm grain size and 100 MPa confining pressure were inferred from Rutter's appendices. Although deformation mechanism maps for minerals are far more speculative than their metallurgical counterparts, it is clear that dislocation-enhanced corrosion can occur over a wide range of the Earth's crust, dependent on the mineral assemblage. Strain-rate domination by DESD would depress the strain-rate contours, which qualitatively agrees with Rutter's (1976) pressure-solution maps for quartz (Fig. 4c) and calcite (Fig. 4d). Superimposition of the proposed DESD fields (stipple, Figs. 4c & d) illustrates the coincidence at the high shear stress and temperature end of the pressure-solution field, and suggests that some textures presently attributed to pressure solution may be due to DESD.

DESD AND POLYCRYSTALS

Given the potential coincidence of conditions for pressure solution and DESD, the purpose of this section is to explore the possibility of textural recognition. Ideally one would prefer to use real rocks, but the application of even well constrained deformation-mechanism maps to such heterogeneous systems would be difficult. Therefore the discussion below examines an idealized aggregate of hypothetical disc-shaped minerals A and B. The relationships among the minerals are changed by varying a state variable and a material property: fluid phase and grain size. The consequent variation in field boundaries are exaggerated for the sake of illustration. The photoelastic solution for two-dimensional discs subjected to loads at two pairs of diametrically opposed and mutually perpendicular points (Frocht 1948, p. 204) is illustrated in principal stress trajectories (Fig. 5a) and maximum shear-stress trajectories (Fig. 5b). For the sake of simplicity, the hypothetical crystals have one set of slip planes, whose orientations are represented in Figs. 6–8. The deformation mechanisms of A and B are assumed to operate independently. Thus the position on the monomineralic map corresponds to the mechanism in this polymineralic assemblage: the Coble-creep field to pressure solution, the DESD field to dislocation enhanced dissolution, and the dislocation-glide and power-law creep fields to ductile deformation. The textural effect of the dominant strain mechanism is represented in Fig. 6: pressure solution in coarse stipple, DESD in fine stipple, ductile deformation in hatch marks.

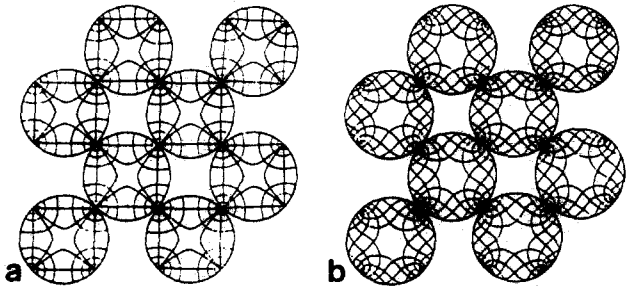

Fig. 5. The photoelastic solution for two-dimensional discs subjected to loads at two pairs of diametrically opposed and mutually perpendicular points (Frocht 1948, p. 204): (a) principal stress trajectories; (b) maximum shear-stress trajectories.

Case 1

Deformation-mechanism maps for 100 μm diameter aggregates of minerals A and B are illustrated in Figs. 6(a) & (b). At 400°C and $10^{2.5}$ MPa, designated by the dots, mineral A deforms by DESD, and mineral B by dislocation-creep. If $\dot{\varepsilon}_A \gg \dot{\varepsilon}_B$, then the DESD of A is the dominant strain mechanism (Fig. 6c). The selective dissolution of dislocations is crystallographically controlled by the magnitude of the shear stress resolved onto the softest slip plane (Meike 1988). Therefore the sites of dissolution are determined by the superimposition of the slip plane geometry onto the maximum shear-stress trajectories (Fig. 5b). Consequently the orientation of only one mineral A grain allows slip, because shear stress resolved on to the slip planes of the other mineral A grains is zero. Thus at this incipient stage only one A grain is subject to DESD. If $\dot{\varepsilon}_A \ll \dot{\varepsilon}_B$ then ductile deformation of B controls the strain of the aggregate (Fig. 6d).

Case 2: *grain size*

In general, a decrease in grain size expands the fields of the boundary mechanisms at the expense of the lattice mechanisms (Mohamed & Langdon 1974). Deformation-mechanism maps for 10 μm diameter aggregates of monomineralic A and B, illustrate this effect (Figs. 7a & b). Under the same conditions as Case 1, 400°C and $10^{2.5}$ MPa, mineral A is in the Coble-creep field. If water is present, this is equivalent to the pressure-solution field of Rutter (1976). Mineral B is in the DESD field. If $\dot{\varepsilon}_A \ll \dot{\varepsilon}_B$ then DESD of B dominates the macroscopic strain (Fig. 7d), and as for mineral A in Case 1, is crystallographically controlled. If $\dot{\varepsilon}_A \gg \dot{\varepsilon}_B$ then the pressure solution of A is the dominant strain mechanism (Fig. 7c). Pressure solution is not crystallographically controlled. Wherever the stress exceeds a threshold value, dissolution occurs because the driving force is the principle stress (Fig. 5a) gradient, not a dislocation gradient. Comparison of DESD (Fig. 6c) and pressure solution (Fig. 7c) suggests that the constraints on the DESD are greater and thus the sites would be less common. This does not imply a slower bulk dissolution rate because reaction energetics may compensate. It does, however, suggest that DESD could be responsible for more anisotropic textures than pressure solution.

Now consider coarse (100 μm) grains of mineral B in a matrix of fine (10 μm) grains of mineral A. If A grains provide the framework, they will control the strain rate of the aggregate. At 400°C and 10^2 MPa Coble creep of A dominates and the resultant texture would appear as the familiar pressure shadow (e.g. Pabst 1931). In con-

trast, at 800°C and 10^3 MPa, DESD of A controls the strain rate. The identification of the mechanism is important to estimate reaction rates as well as timing of events. However microstructural recognition may not be obtainable by standard optical microscopy. In either case the small grains would undergo dissolution and the large grains would exhibit no evidence of the strain mechanism. Clearly the lack of evidence of ductile deformation in the large grain is not proof of pressure solution because the small grains compensate for the strain. Microstructural evidence such as the presence or absence of dislocation gradients and crystallographic control of dissolution could be obtained from higher resolution techniques such as transmission electron microscopy.

Case 3: differential fluid effects

The cases above permit $\dot{\varepsilon}$ to represent all fluid effects. However, two independent effects can be distinguished, one mechanical and the other chemical. Their significance varies from mineral to mineral. For example, hydrolytic weakening has a mechanical effect, and expands the lattice mechanism fields at the expense of the boundary mechanisms. In contrast, dissolution strain is a chemical effect and depends on dissolution rate. In its capacity as a solvent, water expands the boundary-mechanism fields. Both effects increase strain rate and thus depress the strain rate contours. However, whereas the enhancement of dislocation climb could be plotted directly on to a dry aggregate map, a more

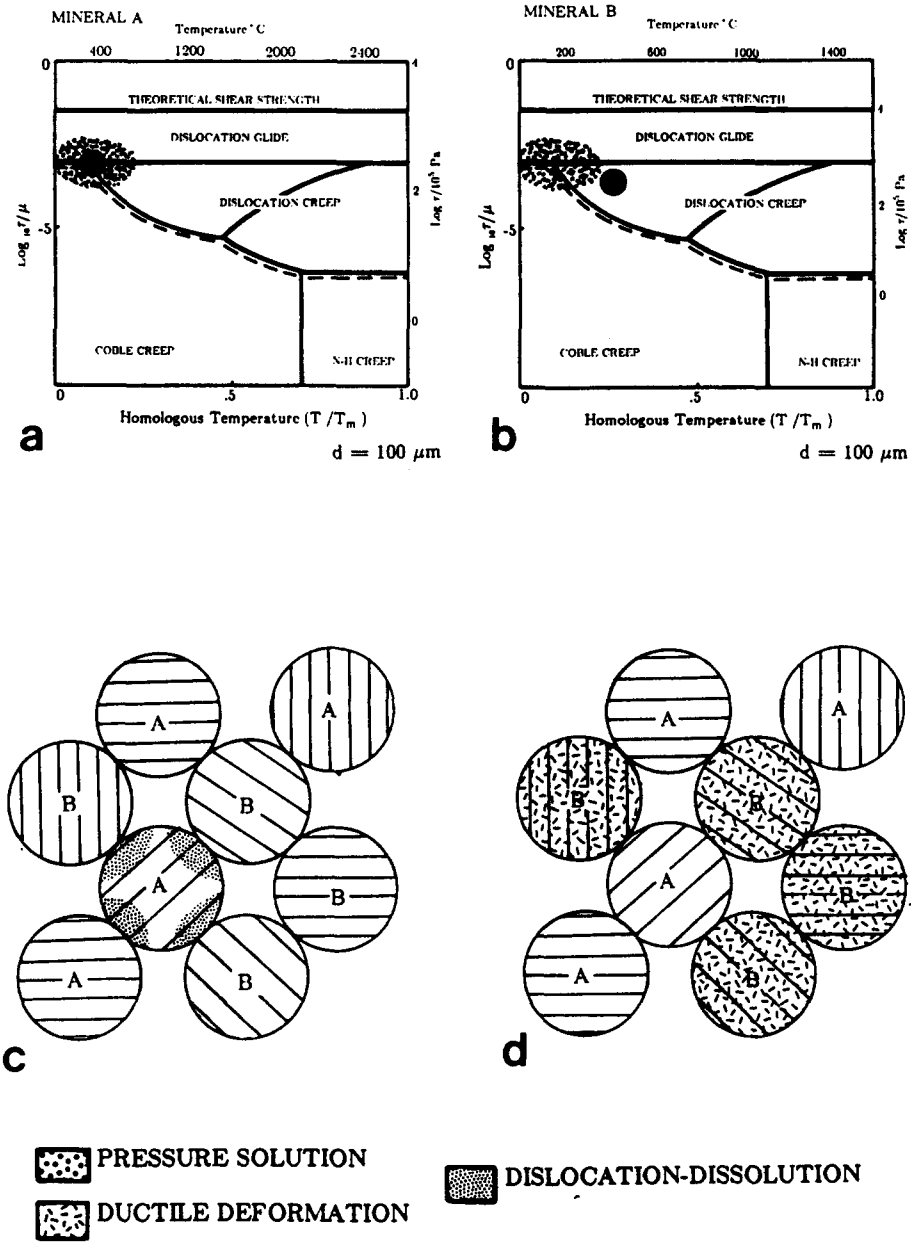

Fig. 6. Diagrams of deformation-mechanism maps at 100 μm diameter for (a) mineral A and (b) mineral B. The ambient conditions for the polymineralic aggregate, 400°C and $10^{2.5}$ MPa are designated by large dots. Textural consequence of strain dominance by (c) DESD of mineral A and (d) dislocation-creep of mineral B. Shaded patterns designated to the three lattice mechanisms under consideration, pressure solution, ductile deformation and DESD are represented below.

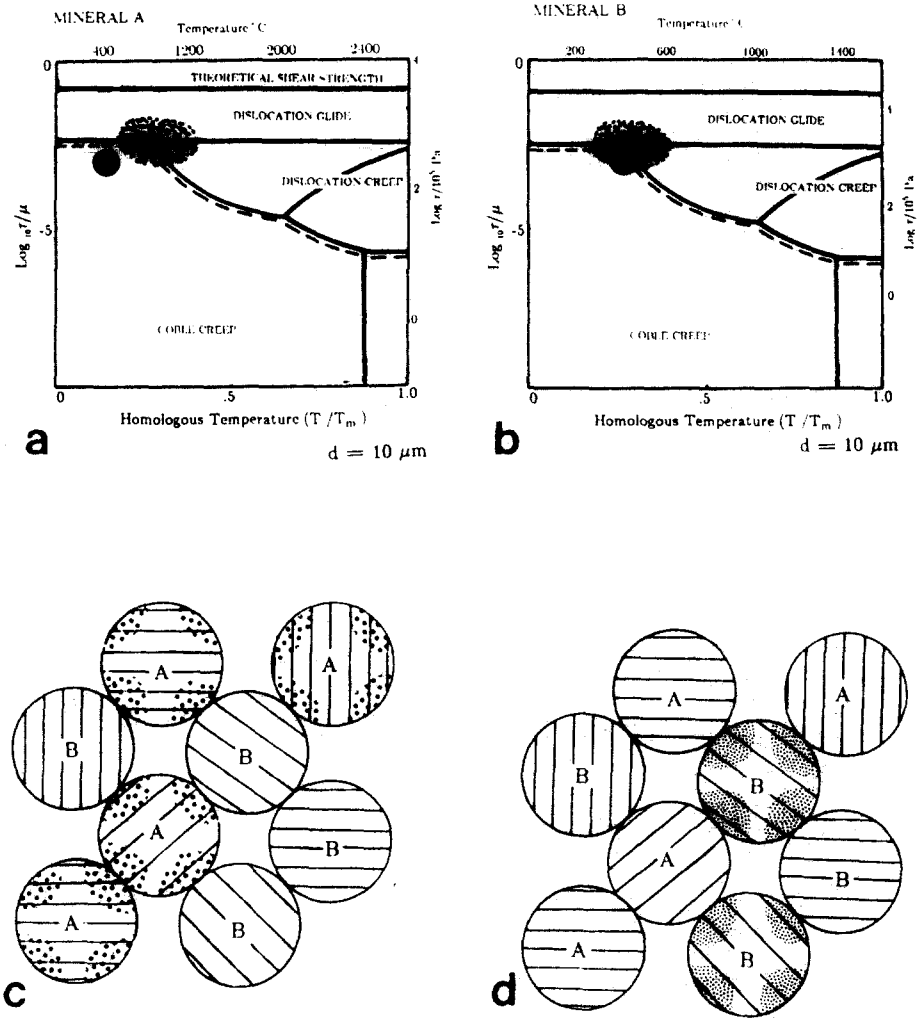

Fig. 7. Diagrams of deformation-mechanism maps at 10 μm diameter for (a) mineral A and (b) mineral B. The ambient condition for the polymineralic aggregate, 400°C and $10^{2.5}$ MPa is designated by large dots. A decrease in grain size expands the fields of the boundary mechanisms at the expense of the lattice mechanisms. Textural consequence of strain domination by (c) pressure solution of mineral A and by (d) DESD of mineral B. Compare the pressure solution of A to the DESD of A (Fig. 6b).

rigorous approach to the chemical effects requires another axis.

Hydrolytic weakening is best documented in quartz (e.g. Hobbs *et al.* 1972, Griggs 1974), but it has also been observed in other minerals (Zabinski 1966, Tullis *et al.* 1979). Suppose water enhances climb in mineral A and expands its lattice mechanism fields (Fig. 8a). Mineral B is not affected and is identical to Case 1 (Fig. 8b). At 400°C and $10^{2.75}$ MPa, both A and B are now ductile. At a lower temperature, 200°C and $10^{2.5}$ MPa, the deformation of mineral A is ductile, and the deformation of B is by DESD. This case is the opposite of the first (Fig. 6). If $\dot{\varepsilon}_A \gg \dot{\varepsilon}_B$ then the ductile deformation of A is the dominant strain mechanism (Fig. 8c). If $\dot{\varepsilon}_A \ll \dot{\varepsilon}_B$, then the DESD of B dominates (Fig. 8d).

Suppose the chemical effect of water on mineral B is significant, comparable to Fig. 7(b), and insignificant for A, which is then identical to Fig. 6(a). At 400°C and $10^{2.5}$ MPa both minerals are found in the DESD field. To demonstrate the complexity of textural interpretation, it is important to note that even if the dislocation microstructures in mineral A and B are identical, one mineral can still control the strain rate. If the dislocation density makes mineral A more unstable than mineral B, the DESD of A controls the strain. Another possibility is that mineral B undergoes a transformation to a metastable phase, and subsequently the metastable phase dissolves more rapidly than deformed crystals of either A or B. As a result, DESD of B controls the macroscopic strain rate.

CONCLUSIONS

An energetic analysis of dislocation microstructures representative of a range of lattice-controlled flow mechanisms indicates that the greatest strain energy is obtained from free dislocations. The strain-energy contribution of a dislocation wall is always less than that of an equal density of free dislocation line, and in the limit approaches zero. The energetic arguments demonstrate the importance of submicroscopic-scale characterization of specimens used in experimental dissolution studies. It is concluded that free dislocation pile-ups most favor

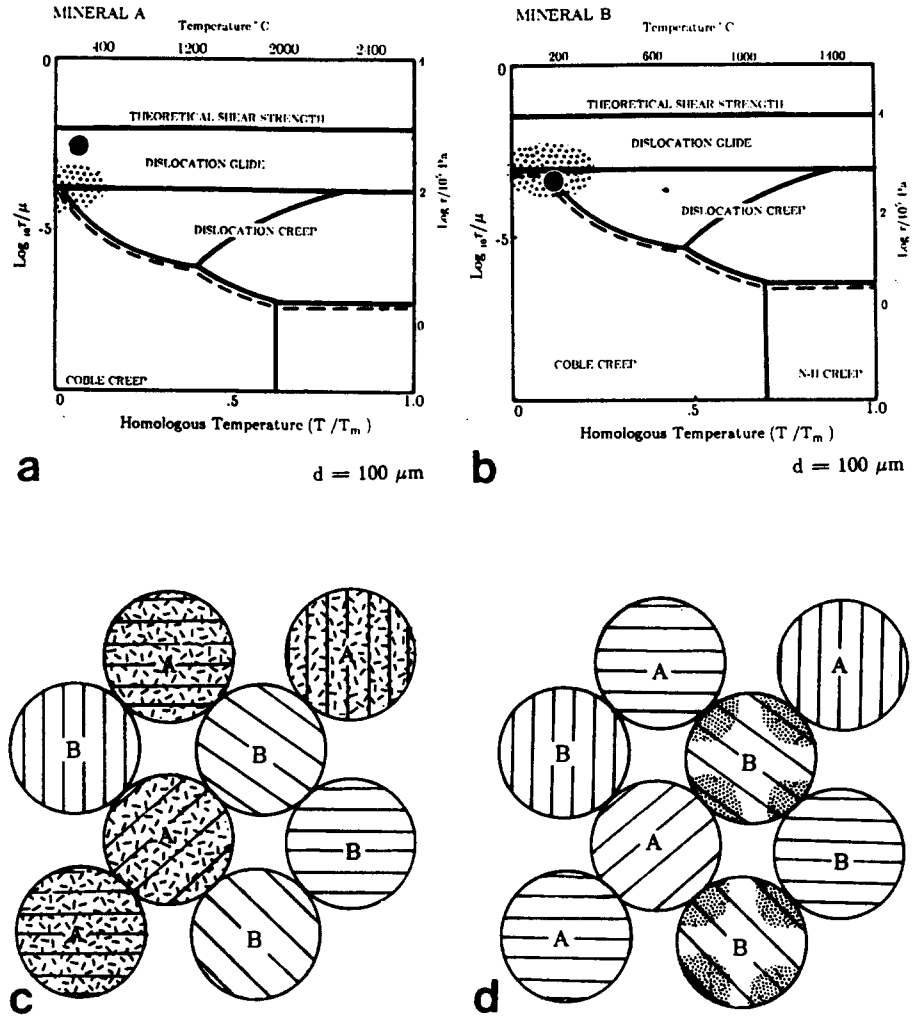

Fig. 8. Deformation-mechanism maps illustrate the mechanical effect of water, expands the lattice-mechanism fields. (a) Water enhances climb in mineral A. (b) Mineral B is not affected. At 400°C and $10^{2.5}$ MPa, both A and B are ductile. The dots designate a temperature of 200°C and $10^{2.75}$ MPa. (c) The deformation of mineral A is ductile. (d) The deformation of B is by DESD. Compare Figs. 6(c) & (d).

selective dissolution. Dynamical arguments suggest that ductile deformation is not required for this DESD microstructure. Ductile strain represents a reduction in the potential for DESD strain, both energetically and in the existence of an alternative mechanism of plastic flow. The limitation suggests that a dislocation-activated reaction field is located on a deformation-mechanism map at low homologous temperature and relatively low homologous shear stress. These limiting conditions are based on micromechanical arguments and therefore apply to any mechanism activated by dislocation-strain energy. A comparison of monomineralic assemblages suggests that the DESD mechanism can occur over a wide range of conditions dependent on the mineral assemblage.

The overlap between the proposed DESD and pressure-solution fields suggests that the two mechanisms may not presently be distinguished. The identity of the mechanism may affect estimates of deformation rates as well as timing of events. An exploration of the textural consequences of DESD and pressure solution in a polymineralic aggregate employs deformation-mechanism maps. The assessment points out that solution-transfer deformation mechanisms are affected by grain size and the mechanical and chemical effects of water as well as the more commonly recognized pressure and temperature. In addition it appears that textures that result from DESD-dominated strain could be distinguished from those that result from pressure-solution strain as described in theory. The crystallographic control of dissolution in the case of DESD provides the potential for more heterogeneous and anisotropic textures.

Acknowledgements—This paper has benefited from the reviews of J. P. Platt, M. S. Paterson, R. P. Wintsch and an unnamed referee. The work was supported by a University of California President's Fellowship and the Director, Office of Energy Research, under contract No. DE-AC03-76SF0098.

REFERENCES

Albrecht, H. & Hunsche, U. 1980. Gebirgsmechanische Aspekte bei der Endlagerung radioaktiver Abfälle in Salzdiapiren unter besonderer Berücksichtigung des Fliessverhaltens von Steinsalz. *Fortschr. Mineral.* **58**, 212–247.

Bacon, D. J. & Martin, J. W. 1982. Computer simulation of dislocation cores in hcp metals. *Phys. Stat. Solid (b)* **114**, 269–279.

Bennema, P. & Van Enckevort, W. J. P. 1979. On the occurrence of a

critical driving force for dissolution: theory and experimental observation on KDP and other crystals. *Ann. Chim.* **4**, 451–459.
Birch, F. 1966. Compressibility; Elastic constants. In: *Handbook of Physical Constants* (edited by Clark, S. P., Jr). *Mem geol. Soc. Am.* **97**, 97–173.
Brantley, S. L., Crane, S. R., Crear, D., Hellman, R. & Stallard, R. 1986. Dissolution at dislocation etch pits in quartz. *Geochim. cosmochim. Acta* **50**, 2349–2361.
Bucher, M. 1982. Core energy and Peierls stress of edge dislocations on {110} and {001} slip planes in NaCl. *Phys. Stat. Solid (b)* **114**, 249–268.
Cabrera, N. & Levine, M. M. 1956. On the dislocation theory of evaporation of crystals. *Phil. Mag.* **1**, 450–458.
Cabrera, N., Levine, M. M. & Plaskett, J. S. 1954. Hollow dislocations and etch pits. *Phys. Rev.* **96**, 1153.
Cahn, R. W. 1985. The discovery of polygonization. In: *Dislocations and Properties of Real Materials*. Institute of Metals, London, 12–14.
Casey, W. H., Carr, M. J. & Graham, R. A. 1988. Crystal defects and the dissolution kinetics of rutile. *Geochim. cosmochim. Acta* **52**, 1545–1556.
Clarebrough, L. M., Hargreaves, M. E. & West, G. W. 1957. The density of dislocations in compressed copper. *Acta metall.* **5**, 738–740.
Coe, R. S. 1970. The thermodynamic effect of shear stress on the ortho-clino inversion in enstatite and other coherent phase transitions characterized by a finite simple shear. *Contr. Miner. Petrol.* **26**, 247–264.
Coe, R. S. & Paterson, M. S. 1969. The α–β inversion in quartz: a coherent phase transition under nonhydrostatic stress. *Phys. Rev.* **7**, 215–223.
Cottrell, A. H. 1953. *Dislocations and Plastic Flow in Crystals*. Oxford University Press, London.
Durney, D. W. 1972. Solution transfer: an important geological deformation mechanism. *Nature Phys. Sci.* **235**, 315–317.
Elliot, D. 1972. Diffusional flow laws in metamorphic rocks. *Bull. geol. Soc. Am.* **84**, 2645–2663.
Frank, F. C. 1951. Capillary equilibria of dislocated crystals. *Acta Crystall.* **4**, 497–501.
Frocht, M. M. 1948. *Photoelasticity, Volume* 1. J. Wiley and Sons, New York.
Frost, H. J. & Ashby, M. F. 1982. *Deformation Mechanism Maps: The Plasticity and Creep of Metals and Ceramics*. Pergamon Press, Oxford.
Green, H. W. 1972. Metastable growth of coesite in highly strained quartz. *J. geophys. Res.* **77**, 2478–2482.
Green, H. W. 1980. On the thermodynamics of non-hydrostatically stressed solids. *Phil. Mag.* A **41**, 637–647.
Griggs, D. 1974. A model of hydrolytic weakening in quartz. *J. geophys. Res.* **79**, 1653–1661.
Helgeson, H. C., Murphy, W. M. & Aagaard, P. 1984. Thermodynamics and kinetic constraints on reaction rates among minerals and aqueous solutions II. Rate constants, effective surface area, and the hydrolysis of feldspar. *Geochim. cosmochim. Acta* **48**, 2405–2432.
Hobbs, B. E., McLaren, A. C. & Paterson, M. S. 1972. Plasticity of single crystals of synthetic quartz. In: *Flow and Fracture of Rocks* (edited by Heard, C., Borg, I. Y., Carter, N. C. & Raleigh, C. B.). AGU, Washington, DC, 29–53.
Kamb, B. 1961. The thermodynamic theory of nonhydrostatically stressed solids. *J. geophys. Res.* **66**, 259–271.
Kerrich, R., Fyfe, W. S., Gorman, B. E. & Allison, I. 1977. Local modification of rock chemistry by deformation. *Contr. Miner. Petrol.* **65**, 183–190.
Kerrick, D. M. 1986. Dislocation strain energy in the Al_2SiO_5 polymorphs. *Phys. Chem. Miner.* **13**, 221–226.
Keyes, R. W. 1958. Dilatational strain due to dislocation in copper. *Acta metall.* **6**, 611–612.
Lasaga, A. C. & Blum, A. 1986. Surface chemistry, etch pits and mineral-water reactions. *Geochim. cosmochim. Acta* **50**, 2363–2379.
McClay, K. R. 1977. Pressure solution and Coble creep in rocks and minerals. *J. geol. Soc. Lond.* **134**, 57–70.
Meike, A. 1988. Heterogeneous strain resulting from stress gradients in calcite single crystals. *Phys. Chem. Miner.* **16**, 148–156.
Meike, A. & Wenk, H. R. 1988. A TEM study of microstructures associated with solution cleavage in limestone. *Tectonophysics* **154**, 137–148.
Mohamed, F. A. & Langdon, T. G. 1974. Deformation mechanism maps based on grain size. *Met. Trans.* **5**, 2339–2345.
Murphy, W. M. 1989. Dislocations and feldspar dissolution. *Eur. J. Mineral.* **1**, 315–326.
Nabarro, F. R. N. 1967. *Theory of Crystal Dislocations*. Oxford University Press, London.
Newton, R. C., Goldsmith, J. R. & Smith, J. V. 1969. Aragonite crystallization from strained calcite at reduced pressures and its bearing on aragonite in low-grade metamorphism. *Contr. Miner. Petrol.* **22**, 335–348.
Pabst, A. 1931. Pressure shadows and the measurement of the orientation of minerals in rocks. *Am. Miner.* **16**, 55–70.
Paterson, M. S. 1973. Nonhydrostatic thermodynamics and its geological applications. *Rev. Geophys. & Space Phys.* **11**, 355–389.
Peierls, R. 1940. The size of a dislocation. *Proc. Phys. Soc. Lond.* **52**, 34–37.
Poirier, J.-P. 1981. Martensitic olivine-spinel transformation and plasticity of the mantle transition zone. In: *Anelastic Properties and Related Processes in the Earth's Mantle. Am. Geophys. Un. Geodyn. Ser.* **4**, 113–117.
Poirier, J.-P. 1985. *Creep of Crystals*. Cambridge University Press, London.
Porter, D. A. & Easterling, K. E. 1982. *Phase Transformations in Metals and Alloys* (2nd printing). Van Nostrand Reinhold Co. Ltd., Wokingham, U.K.
Puls, M. P. 1981. Atomic models of single dislocations. In: *Dislocation Modelling of Physical Systems* (edited by Ashby, M. F., Bullough, R., Hartley, C. S. & Hirth, J. P.). Pergamon Press, New York, 249–268.
Rutter, E. H. 1976. The kinetics of rock deformation by pressure solution. *Phil. Trans. R. Soc. Lond.* A **283**, 203–219.
Schmid, E. 1924. 'Yield point' of crystals. Critical shear stress law. *Proceedings of the International Congress on Applied Mechanics*. Delft, Holland.
Smith, B. K. 1982. Plastic deformation of garnets: mechanical behavior and associated microstructures. Unpublished Ph.D. Dissertation, University of California, Berkeley.
Sorby, H. C. 1863. On the direct correlation of mechanical and chemical forces. *Proc. R. Soc.* **12**, 538–550.
Stocker, R. L. & Ashby, M. F. 1973. On the rheology of the upper mantle. *Rev. Geophys. & Space Phys.* **11**, 391–426.
Tullis, J., Shelton, G. L. & Yund, R. A. 1979. Pressure dependence of rock strength: implications for hydrolytic weakening. *Bull. Mineral.* **102**, 110–114.
Van der Hoek, B., Van der Eerden, J. P. & Bennema, P. 1982. Thermodynamical stability conditions for the occurrence of hollow cores caused by stress of line and planar defects. *J. Crystal Growth* **56**, 621–632.
Vaughan, P. J., Green, H. W. & Coe, R. S. 1984. Anisotropic growth in the olivine-spinel transformation of Mg_2GeO_4 under nonhydrostatic stress. *Tectonophysics* **108**, 299–322.
Weyl, P. K. 1959. Pressure solution and the force of crystallization—a phenomenological theory. *J. geophys. Res.* **64**, 2001–2025.
Wintsch, R. P. & Dunning, J. 1985. The effect of dislocation density on the aqueous solubility of quartz and some geologic implications: a theoretical approach. *J. geophys. Res.* **90**, 3649–3657.
Zabinski, W. 1966. Hydrogarnets. *Pol. Akad. Nauk Oddzial Krakowie Kom., Nauk Mineral.* **3**, 1–61.